X-641-73-230
PREPRINT

NASA TM X- 70445

SHAPED SCINTILLATION DETECTOR SYSTEMS FOR MEASUREMENTS OF GAMMA RAY FLUX ANISOTROPY

J. I. TROMBKA
J. I. VETTE
F. W. STECKER
E. L. ELLER
W. T. WILDES

AUGUST 1973

GSFC
GODDARD SPACE FLIGHT CENTER
GREENBELT, MARYLAND

SHAPED SCINTILLATION DETECTOR SYSTEMS FOR MEASUREMENTS OF GAMMA RAY FLUX ANISOTROPY

J. I. Trombka

J. I. Vette

F. W. Stecker

E. L. Eller

W. T. Wildes

Goddard Space Flight Center

Greenbelt, Maryland 20771

SHAPED SCINTILLATION DETECTOR SYSTEMS FOR

MEASUREMENTS OF GAMMA RAY FLUX ANISOTROPY

Abstract

The detection efficiencies of cylindrical detectors for various gamma ray photon angular distributions have been studied in the energy range from .10 Mev to 15 Mev. These studies indicate that simple detector systems on small satellites can be used to measure flux anistropy of cosmic γ-rays and the angular distribution of albedo gamma rays produced in planetary atmospheres. The results indicate that flat cylindrical detectors are most suitable for measuring flux anisotropy because of their angular response function. A general method for calculating detection efficiencies for such detectors is presented.

Page intentionally left blank

CONTENTS

SHAPED SCINTILLATION DETECTOR SYSTEMS FOR MEASUREMENTS OF GAMMA RAY FLUX ANISOTROPY

1. Introduction

Recent observations of cosmic gamma rays and theoretical studies of their implications have indicated that observational data in the 0.3 MeV to 30 MeV energy range may provide important cosmological information about the early history of our universe.[1-7] Cosmic gamma-rays in this energy range are expected to be highly isotropic and thus of cosmological origin. A direct observational test of the isotropy of the flux can be an extremely sensitive test of cosmological origin and such a measurement may provide a determination of the strength of galactic gamma-ray emission in 0.3 to 30 MeV energy region. Detailed spectral information in this energy range will provide important information as to the nature and origin of the gamma-radiation.

It may be possible to study the structure of a planet's atmosphere by measuring the energy and angular distribution of the albedo gamma-rays. Such measurements will also be considered in this paper.

We present here the results of an investigation of the properties of cylindrical detectors which can be used to optimize the design of simple systems for performing the following measurements:

1. The gamma-ray flux anisotropy.
2. The possible presence of point sources.

2. Definitions of Effective Cross Sectional Area and Intrinsic Detection Efficiency

The response of a particular detector system can be evaluated in terms of a detection efficiency which depends on the geometry of the system and upon the spatial and angular distribution of the incident flux being measured. Because source to detector distances in astronomical measurements are very much greater than detector dimensions, spatial variations over the detector may be ignored. We will use a rectangular coordinate system (x', y', z') fixed in the detector to describe positions within the volume of the detector system. We will denote a spatially fixed coordinate system by the unprimed rectangular coordinates (x, y, z) and use (b, ℓ) for the latitude and longitude angles. When one considers the application of the results derived in this section to gamma ray astronomy, the most convenient unprimed system will be the galactic system. The angles (b, ℓ) will be used to describe the direction of the incident photons. The orientation of the detector system will be specified by giving the latitude and longitude of the z' and x' axes denoted by $b_{z'}$, $\ell_{z'}$, and $b_{x'}$, $\ell_{x'}$, respectively.

The geometry of a general situation is given in Figure 1. The x' and y' axes are not included in order to show more clearly the various angles and a photon flux from direction (b, ℓ) entering the detector at point A (x', y', z'). The rectilinear path through the crystal along the incident photon direction is denoted by $\overline{AB}$ with a distance ξ. We will denote the photon flux which is differential in angle and energy by the quantity

$$f(E,\ b,\ \ell) = \frac{d^2F}{d\Omega}\ dE \tag{1}$$

where

$$d\Omega = d(\sin b)\ d\ell. \tag{2}$$

We can then compute C, the total number of photons per unit time and energy which will interact with the detector, by

$$C(E,\ b_{z'},\ \ell_{z'}, b_{x'},\ \ell_{x'}) = \int_{\Omega}\int_{S'} f(E,\ b,\ \ell)$$
$$\{1 - \exp[-\mu(E)\,\xi\,(b_{z'},\ \ell_{z'},\ b_x,\ \ell_{x'},\ x',\ y',\ z',\ b,\ \ell]\}\ dA_{\perp}\ d\Omega, \tag{3}$$

where $dA_{\perp}$ is the element of detector surface area perpendicular to the direction (b, ℓ) at the point of entry A (x', y', z') and S' represents the integration over the surface of the detector where photons enter. The quantity μ is the linear absorption coefficient which is energy dependent and represents the sum of the photoelectric, Compton, and pair production interactions. The quantity within the braces represents the probability that the photon will have at least one interaction within the crystal. Multiple interactions occur in times shorter than the decay of the scintillation produced in the detector and thus appear as a single interaction. These multiple interactions will change the amount of energy deposited in the crystal but not intrinsic efficiency.

The effective detector cross sectional area is defined as:

$$\eta = \frac{C}{\int_{\Omega} f\,d\Omega} \tag{4}$$

and the intrinsic detection efficiency as:

$$\epsilon = \frac{C}{\int_{\Omega} \int_{S'} f \, d\Omega dA_{\perp}} . \tag{5}$$

The variability of ϵ as a function of energy for three special flux distribution is illustrated in Figure 2 for a relatively symmetric crystal 10.16 cm long × 10.16 cm in diameter. More extreme shapes most likely will show greater differences because of increased proportions of short path lengths for an isotropic flux. Therefore, the quantities η and ϵ are not useful in the case of an unknown photon distribution. They are also difficult to calculate for irregular detector geometries, but special cylindrical cases which are useful will be examined.

3. Response of a Cylindrical Detector to a Parallel Beam

We now specialize the geometry of the crystal to a right cylinder of height, H, and radius, R, with z' as the axis of symmetry and consider the flux distribution to be a plane wave coming from direction (b_0, ℓ_0). We do the plane wave case first since the results for a planar and an isotropic flux can be calculated in terms of the plane wave case. For a plane wave

$$f = P(E) \, \delta (\sin b - \sin b_0) \, \delta (\ell - \ell_0) \tag{6}$$

Since we have cylindrical symmetry, the only angle of importance is the one between z' and the direction of the photon beam. We will denote this angle by θ and it is given in terms of (b_0, ℓ_0) and $(b_{z'}, \ell_{z'})$ by

$$\cos \theta = \cos b_0 \cos b_{z'} \cos (\ell_0 - \ell_{z'}) + \sin b_0 \sin b_{z'}, \tag{7}$$

and P(E) has units of photons/cm^2-sec-MeV. In this case we obtain

$$\eta(E,\theta) = 2RH \sin\theta \left\{1 - \int_0^{\pi/2} \cos\beta \left[\exp - \left(\frac{2\mu R \cos\beta}{\sin\theta}\right)\right] d\beta\right\}$$

$$+ \pi R^2 \cos\theta \left\{1 + \frac{4}{\pi} \int_0^{\pi/2} \cos^2\beta \left[\exp - \left(\frac{2\mu R \cos\beta}{\sin\theta}\right)\right] d\beta\right\}$$

$$- \frac{4R}{\mu} \sin\theta \cos\theta \left\{1 - \int_0^{\pi/2} \cos\beta \left[\exp - \left(\frac{2\mu R \cos\beta}{\sin\theta}\right)\right] d\beta\right\} \quad (8)$$

for $\tan\theta \geq 2R/H$, and

$$\eta(E,\theta) = 2RH \sin\theta \left\{1 - \int_\alpha^{\pi/2} \cos\beta \left[\exp - \left(\frac{2\mu R \cos\beta}{\sin\theta}\right)\right] d\beta + \sin\alpha \left[\exp - \left(\frac{2\mu H}{\cos\theta}\right)\right]\right\}$$

$$+ \pi R^2 \cos\theta \left\{1 + \frac{4}{\pi} \int_\alpha^{\pi/2} \cos\beta \left[\exp - \left(\frac{2\mu R \cos\beta}{\sin\theta}\right)\right] d\beta - \frac{2}{\pi}\left(\alpha + \frac{\sin 2\alpha}{2}\right)\left[\exp - \left(\frac{2\mu H}{\cos\theta}\right)\right]\right\}$$

$$- \frac{4R}{\mu} \sin\theta \cos\theta \left\{1 - \int_\alpha^{\pi/2} \cos\beta \left[\exp - \left(\frac{2\mu R \cos\beta}{\sin\theta}\right)\right] d\beta - \sin\alpha \left[\exp - \left(\frac{2\mu H}{\cos\theta}\right)\right]\right\} \quad (9)$$

for $\tan\theta \leq 2R/H$, where $\cos\alpha = H/2R \tan\theta$ and $\cos\beta = \xi/2R$.

The intrinsic detection efficiency is then given by

$$\epsilon_p(\theta) = \frac{\eta_p(\theta)}{2RH \sin\theta + \pi R^2 \cos\theta}. \quad (10)$$

This case is useful when one is dealing with a single distant point source since the detector counting rate will be given by

$$C_{ps}(E, \theta) = \eta_p(E, \theta)\, P(E) \tag{11}$$

for a given energy photon E and by

$$C_{ps}(\geq E_T, \theta) = \int_{E_T}^{\infty} \eta_p P(E)\, dE \tag{12}$$

for all photons above a threshold energy E_T.

4. Response of a Cylindrical Detector to a Planar Flux

For simplicity of calculation we consider the planar or disc like flux to lie in the plane b = 0. In this case

$$f = J(E)\, \delta(\sin b) \tag{13}$$

and J has units of photons/cm^2 -sec-MeV-rad. We wish to consider only two orientations of the cylindrical detector. Case 1: The z' axis lies in the plane b = 0 (i.e., $\vec{z} \cdot \vec{z}' = 0$). Case 2: The z' axis is perpendicular to this plane (i.e., $\vec{z} \cdot \vec{z}' = |\vec{z}|\,|\vec{z}|$). For Case 1, we find from (7) that

$$\theta = \ell - \ell_{z'},$$

and we can choose $\ell_{z'} = 0$ without loss of generality. Then we have, by performing the integration in (3),

$$C_J(E, b_{z'} = 0) = J(E) \int_0^{2\pi} \eta_p(E, \theta)\, d\theta \tag{14}$$

Since

$$\int f \, d\Omega = 2\pi J(E) \tag{15}$$

and

$$\int_{\Omega} \int_{S'} f \, d\Omega dA_{\perp} = 4 [2RH + \pi R^2] \; J(E) \tag{16}$$

we obtain

$$\eta_J (E, \; b_{z'} = 0) = \frac{2}{\pi} \int_0^{\pi/2} \eta_p (E, \; \theta) \; d\theta \tag{17}$$

and

$$\epsilon_J (E, \; b_{z'} = 0) = \frac{\int_0^{\pi/2} \eta_p (E, \; \theta) \; d\theta}{[2RH + \pi R^2]}. \tag{18}$$

For certain purposes, it is useful to define an effective geometric factor in this case by

$$G_J (E, \; b_{z'} = 0) = \frac{C}{J(E)} = 4 \int_0^{\pi/2} \eta_p (E, \; \theta) \; d\theta \tag{19}$$

We note that G_J has units of cm^2-rad. For the 2nd case we have from (7) that $\theta = \pi/2$ and it follows that

$$C_J (E, \; b_{z'} = \pi/2) = 2\pi J(E) \; \eta_p (E, \; \pi/2), \tag{20}$$

$$\eta_J (E, \; b_{z'} = \pi/2) = \eta_p (E, \; \pi/2), \tag{21}$$

$$\int_{\Omega} \int_{S'} f \, d\Omega dA_{\perp} = 4\pi RHJ(E), \tag{22}$$

$$\epsilon_J(E,\ b_{z'} = \pi/2) = \frac{\eta_p(E,\ \pi/2)}{2RH}, \tag{23}$$

and

$$G_J(E,\ b_{z'} = \pi/2) = 2\pi\eta_p(E,\ \pi/2). \tag{24}$$

5. Response of a Cylindrical Detector to an Isotropic Flux

In the case of an isotropic flux

$$f(b,\ \ell,\ E) = I(E), \tag{25}$$

where I(E) has units of photons/cm^2-sec-MeV-ster. For simplicity of calculation and without any loss of generality we take the (x', y', z') system exactly coincident with the (x, y, z) system. Then we find from (7) that $\theta = \pi/2 - b_0$ and

$$C_I(E) = 4\pi I(E) \int_0^{\pi/2} \eta_p(E,\ \theta)\ d(\cos\theta), \tag{26}$$

$$\eta_I(E) = \int_0^{\pi/2} \eta_p(E,\ \theta)\ d(\cos\theta), \tag{27}$$

$$\int_\Omega \int_{S'} f\, d\Omega dA_\perp = 2\pi^2 RI(H + R), \tag{28}$$

and

$$\epsilon_I(E) = \frac{2}{\pi R(H + R)} \int_0^{\pi/2} \eta_p(E,\ \theta)\ d(\cos\theta). \tag{29}$$

In this case we also define an effective geometrical factor by

$$G_I(E) = \frac{C_I(E)}{I(E)} = 4\pi \int_0^{\pi/2} \eta_p(E, \theta)\, d(\cos\theta) \qquad (30)$$

and G_I has units of cm^2-ster.

6. Measurement of Cosmic Gamma Ray Flux Anisotropy with a Cylindrical Crystal

The effective geometry factors, $G_J(E, O)$, $G_J(E, \pi/2)$ and $G_I(E)$ can be used to show how the anisotropy of the cosmic gamma ray flux in the energy range 1-10 MeV can be measured or have a sensitive upper limit placed on it.

If the flux is not isotropic, the most likely source of excess photons will be from the galactic plane. We consider a spinning satellite placed in an orbit such that it spends a considerable fraction of its time away from the particle radiation environment near the earth and has its spin axis in the galactic plane. Spallation effects produced by cosmic rays in NaI and CsI crystals are not considered, although they have been shown (Reference 11, 12) to be an important background in determining the true cosmic gamma ray flux. However, these will not interfere with the measurement of the flux from the galactic plane by this method, but will increase the background and the error in the determination of anisotropy.

A flat cylindrical (disc) crystal placed in the spinning satellite with a diameter lying in the spin axis will result in a motion such that the z' axis will spend some of its time perpendicular to the galactic plane and some of its time in the galactic plane. We show later that a disc is better than a rod for a given mass detector.

We denote the total amount of time spent in each position to be T; then the total counts per unit energy will be for the case of z' perpendicular to the galactic plane

$$C_{\perp}(E) = \left[I(E)\, G_I(E) + J(E)\, G_J\left(E, \frac{\pi}{2}\right)\right] T \tag{31}$$

and for the case z' parallel to the galactic plane

$$C_{\parallel}(E) = [I(E)\, G_I(E) + J(E)\, G_J(E, 0)] \cdot T. \tag{32}$$

These can be solved for J(E) and I(E) to obtain

$$J = \frac{(C_{\parallel} - C_{\perp})}{\left[G_J(E, 0) - G_J\left(E, \frac{\pi}{2}\right)\right]}, \tag{33}$$

and if we assume that $I >> J$

$$I = \frac{1}{G_I T}\left\{C_{\parallel} - \frac{(C_{\parallel} - C_{\perp})\, G_J(E, 0)}{\left[G_J(E, 0) - G_J\left(E, \frac{\pi}{2}\right)\right]}\right\} \approx \frac{C_{\parallel}}{G_I T} \approx \frac{C_{\perp}}{G_I T} \tag{34}$$

We know from experimental evidence that J is small in the energy range of interest and therefore $C_{\perp} \approx C_{\parallel}$. We will define a geometrical sensitivity factor for a monoenergetic flux by the quantity

$$S' = \frac{G_J(E, 0) - G\left(E, \frac{\pi}{2}\right)}{G_I(E)} \tag{35}$$

and the effective anisotropy by the quantity

$$\delta = \frac{2\pi J}{4\pi I} = \frac{J}{2I} \tag{36}$$

Since $I = I_{TRUE}$ + Background, we cannot measure true anisotropy by this method. The effective anisotropy will be less than the true anisotropy. With this understanding, we can write

$$\delta = \frac{C_{\parallel} - C_{\perp}}{2C_{\perp}} \frac{1}{S'} . \tag{37}$$

The statistical error (i.e. standard deviation) in δ is

$$\sigma_{\delta} = \frac{1}{2S'} \left[\frac{(C_{\parallel} + C_{\perp})^{1/2}}{C_{\perp}} - \frac{(C_{\parallel} - C_{\perp}) C_{\perp}^{1/2}}{C_{\perp}^2} \right] \approx \frac{1}{S'} \sqrt{\frac{1}{2C_{\perp}}} , \tag{38}$$

since $C_{\parallel} \approx C_{\perp}$. Then if we use the criterion that the minimum measureable quantity must be 3 times the standard deviation, the smallest value of δ that can be observed is

$$\delta_{min} = 3\sigma_{\delta} = \frac{3}{S'} \sqrt{\frac{1}{2C_{\perp}}} . \tag{39}$$

Now to write this in terms of I and T, we use (34) to obtain

$$\delta_{min} = \frac{3}{S'} \sqrt{\frac{1}{2IG_I T}} = \frac{3}{S} \sqrt{\frac{1}{2IT}} , \tag{40}$$

where

$$S = S' \sqrt{G_I} = \frac{G_J(E, 0) - G_J\left(E, \frac{\pi}{2}\right)}{\sqrt{G_I}} . \tag{41}$$

Thus for a fixed value of I, one can decrease the minimum measureable value of δ by making $|S|$ as large as possible and by increasing T.

In the case of an integral spectrum we can follow a similar analysis by starting with (31) and (32) and integrating over E.

$$C_{\perp}(>E) = \left[\int_E^{\infty} I(E)\, G_I(E)\, dE + \int_E^{\infty} J(E)\, G_J\left(E, \frac{\pi}{2}\right) dE\right] T \qquad (42)$$

$$C_{\parallel}(>E) = \left[\int_E^{\infty} I(E)\, G_I(E)\, dE + \int_E^{\infty} J(E)\, G_J(E, 0)\, dE\right] T \qquad (43)$$

Another useful quantity can be obtained from rewriting equations (42) and (43) in the following way

$$C_{\perp}(>E) = \bar{G}_I \int_E^{\infty} I(E)\, dE + \bar{G}_J\left(\frac{\pi}{2}\right)\int_E^{\infty} J(E)\, dE \qquad (42a)$$

$$C_{\parallel}(>E) = \bar{G}_I \int_E^{\infty} I(E)\, dE + \bar{G}_J(0) \int_E^{\infty} J(E)\, dE, \qquad (43a)$$

where

$$\bar{G}_I = \frac{\int_E^{\infty} G_I\, I(E)\, dE}{\int_E^{\infty} I(E)\, dE}, \qquad (44)$$

$$\bar{G}_J\left(\frac{\pi}{2}\right) = \frac{\int_E^{\infty} G_J\left(E, \frac{\pi}{2}\right) J(E)\, dE}{\int_E^{\infty} J(E)\, dE}, \qquad (45)$$

and

$$\overline{G}_J(0) = \frac{\int_E^\infty G_J(E, 0)\, J(E)\, dE}{\int_E^\infty J(E)\, dE}. \tag{46}$$

These average values of the G's can then be used to determine the sensitivity factor S and S' for particular spectral distributions of interest.

To illustrate some points we consider the case of an opaque detector i.e., $\mu \to \infty$. In this case, we see from equation (8) and (9) that

$$\eta_P(\theta) = 2RH \sin\theta + \pi R^2 \cos\theta.$$

This means that

$$G_J(0) = 4R[2H + \pi R], \tag{47}$$

$$G_J\left(\frac{\pi}{2}\right) = 4\pi RH, \tag{48}$$

$$G_I = 2\pi^2 R(H + R), \tag{49}$$

and

$$S = \frac{2\sqrt{2}R\left[1 - \left(\frac{\pi - 2}{\pi}\right)\alpha\right]}{\sqrt{\alpha + 1}}, \tag{50}$$

where $\alpha = H/R$.

If S = 0, the detector will have no sensitivity to flux anisotropy for the two orientations considered above. From equation (50), S will be zero for

$$\alpha = \frac{\pi}{\pi - 2} \simeq 2.75$$

or

$$H \simeq 2.75R$$

Thus for the limiting case of an opaque crystal, when the height becomes somewhat greater than the crystal diameter, the ability to detect flux anisotropy by a rotating crystal becomes very small.

The sensitivity factor S for CsI is shown as a function of height for a number of crystal radii in Figure 3 for $\mu = 4$ ($\sim$ .15 MeV), in Figure 4 for $\mu = .4$ ($\sim$.56 MeV), and in Figure 5 for $\mu = .165$ ($\sim$ 3 MeV to 7 MeV).

The choice of crystal size for maximum sensitivity to the proposed flux anisotropy can be determined from such sensitivity curves. The curves tend to indicate maxima for the higher energy gamma radiation (Figure 4 and 5). Although not shown in the figures, it has been found that for a given volume (mass) of crystal, it is better in terms of sensitivity to use a disc ($2R > H$) rather than rod ($H > 2R$).

As an example, the results of calculations of the minimum measureable δ for a 2 inch thick by 8 inch diameter CsI crystal are presented. For this case the isotropic gamma ray spectrum (approximated by $I = .024E^{-1.7}$) between .3

and 10 MeV as measured by one experiment on Apollo 15 (Reference 7) was used. A power law spectrum with a variable exponent was used for the planar flux. The results are not sensitive to this exponent for spectra harder than an index of minus 2. $\bar{G}_I$, $\bar{G}_J$ (O), and $\bar{G}_J$ ($\pi/2$) were calculated for these spectral distributions. A flight time of 90 days was assumed with a 10 percent duty time in each orientation with respect to the planar flux. Using equations (40) and (44) yields the minimum effective anisotropy which can be measured by the system of .00038. Using equation (36) and the isotropic flux yield a total planar intensity in the .3 to 10 MeV range of 5.5×10^{-5} photons/cm^2-rad-sec for differential energy spectrum with a minus 1 exponent.

7. Measurement of Sources in the Galactic Plane

One can examine the use of this simple system for the detection of sources in the galactic plane. Essentially, the detection efficiency, η_P , (E, θ), in equations 8 and 9 reflects the detector's response as a function of phase angle θ (i.e., the angle between the direction of the source and the cylindrical crystal axis). Figure 6 is a polar plot of the ratio

$$\frac{\eta_p (E, \theta)}{\eta_p \left(E, \frac{\pi}{2}\right)}$$

as a function of phase angle θ for a 40.64 cm × 2.54 cm CsI right cylindrical crystal. The calculation was made for approximately 4 MeV gamma rays. Maximum sensitivity is obtained with the face of the crystal pointing toward the source ($\theta = 0$). As one rotates the crystal the count rate decreases until $\theta = \pi/2$.

The count rate decreases by a factor of 4.5, with the greatest change occuring near minimum. Thus, a source would be better noticed by the minimum rather than the maximum in count rate. We can define an aperture or angular resolution as the width in degrees at half the counting rate. The angular resolution of this system would be $\sim 18°$.

The sensitivity of the system to the detection of point sources is obtained by calculating the expected count for $\theta = 0$ and $\theta = \pi/2$ with respect to the source in the presence of the isotropic flux considered in the previous section. The total expected counts, C_1, for $\theta = 0$ would be

$$C_1 = T\left[\int_E I\eta_I \, dE + \int_E P\eta_p (E, 0) \, dE\right],$$

where P is the parallel beam flux due to the source in photons/cm^2-sec-MeV. The total expected counts for $\theta = \pi/2$ would be

$$C_2 = T\left[\int_E I\eta_I \, dE + \int_E P\eta_p \left(E, \frac{\pi}{2}\right) dE\right].$$

We now define

$$\bar{I} = \int_E I \, dE,$$

$$\bar{P} = \int_E P \, dE,$$

$$\bar{\eta}_I = \frac{\int_E I\eta_I \, dE}{\bar{I}},$$

and

$$\bar{\eta}_p(\theta) = \frac{\int_E P\eta_p(\theta)\, dE}{\bar{P}}$$

Then the point source strength averaged over energy can be found from the difference in counting rate and known average crystal properties by

$$\bar{P} = \frac{C_1 - C_2}{\left[\bar{\eta}_p(0) - \bar{\eta}_p\left(\frac{\pi}{2}\right)\right] T}. \tag{51}$$

The standard deviation, σ_ρ of $\bar{P}$ for weak sources is

$$\sigma_\rho \simeq \sqrt{2\bar{I}\eta_I t} \cdot \frac{1}{\left[\bar{\eta}_p(0) - \bar{\eta}_p\left(\frac{\pi}{2}\right)\right]} \tag{52}$$

For detectability, again we require that

$$\bar{P}_{min} \geq 3\sigma_p = 3\sqrt{\frac{\bar{I}}{T}}\left[\frac{\sqrt{\bar{\eta}_I}}{\bar{\eta}_p(0) - \bar{\eta}_p\left(\frac{\pi}{2}\right)}\right] \tag{53}$$

Assuming an integrated omnidirectional flux, $\bar{I}$ of 7.2×10^{-2} photons/cm^2 -sec-ster and a measurement time of $T = 2.6 \times 10^5$ sec in each position (similar to the situation discussed previously), $\bar{P}_{min} \geq 4 \times 10^{-4}$ photons/cm^2-sec, could theoretically be detected. Galactic sources such as the Crab Nebula are about an order of magnitude greater than this. Systematic errors can, of course, decrease this sensitivity.

8. Measurement of Atmospheric Albedo Gamma Ray Distribution

This methodology of reducing calculations to integrations over the parallel beam case can be applied to more general flux distributions than planar or point sources. An example is the atmospheric albedo gamma ray flux. For this case the space coordinates are such that the z axis extends from the detector to the nadir. The flux is considered to be independent of ℓ. Calculations are done for a monoenergetic flux.

The albedo is much greater than the cosmic flux, so the isotropic background is not important in this case. The main concern here is the detailed variation of the counting rate with detector orientation. Equations (8) and (9) are again used to define η. Using equation (7) to define θ in terms of the flux and detector orientation angles, the counting rate for a given orientation can be written as,

$$C(E, b_{z'}) = \int_0^{2\pi} \int_{\pi}^{b_{max}} \eta_k(E, \ell - \ell_{z'}, b_{z'}, b)\, K(b)\, db\, d(\ell - \ell_{z'}).$$

The independence of C to $1_{z'}$, is a result of the flux symmetry. The relative counting rates for a specific size crystal are given in Figure 7 for various assumed angular distributions. Two different limb angles corresponding to different altitudes for the detector are shown. At higher energies Stecker (Reference 8) has proposed a model for and calculated the scanning angle distribution of albedo gamma rays. This distribution was found by Stecker to be well approximated by a secant up to about 50°. It was found that a disc shaped detector gave a greater variation in counting rate for this model than an equal

volume (mass) rod shaped detector. In addition the disc gives a better differentiation between different exponents of the secant. It can be seen that if the limb angle is known the departure from a secant distribution at the medium energies (3-10 MeV) can be determined with a disc shaped detector.

9. Summary

The cases which have been described involve either determining the intensity of a particular flux in a predetermined background or descriminating among a limited number of flux distributions. The general formulae can be used to describe any flux distributions which can be reduced to integrations over parallel beams if an iterative scheme is used. Iteration is necessary because the quantities η and ϵ used to calculate the flux from the counting rate are themselves dependent on the flux distribution. After the first analysis of the data the efficiencies can be redetermined in order to calculate the flux distribution again, and so forth.

We feel, therefore, that a flat cylindrical crystal in a small satellite to keep local background problems to a minimum is a viable system for studying gamma ray flux distributions from orbit.

10. References

1. J. R. Arnold, A. E. Metzger, E. C. Anderson, and M. A. Van Dilla, J. Geophys. Res. 67, (1962), 4878.

2. J. I. Vette, D. Gruber, J. L. Matteson, and L. E. Peterson, Proc. I.A.U. Symp. No. 37 (L. Gratton, editor), Reidel Pub. Co., Dordrecht, Holland, 1970, 335.

3. H. A. Mayer-Hasselwander, E. Pfefferman, K. Pinkau, H. Rothermel, and M. Sommer, Ap. J. (Letters) 175, 1972, L23.

4. G. H. Share, R. L. Kinzer, and N. Seeman, Proc. IAU Symp. No. 55 (Reidel in press).

5. C. E. Fichtel, Bull. Am. Phys. Soc. 1973, Ser. II, Vol. 18, No. 4, p. 711.

6. F. W. Stecker, Nature, 241, (1973), 74-77.

7. J. I. Trombka, A. E. Metzger, J. R. Arnold, J. L. Matteson, R. C. Reedy, and L. E. Peterson, Astrophys. J., 181 (1973), 737-746.

8. F. W. Stecker, Nature 242, (1973), 59-60.

9. J. I. Trombka, F. Senftle, R. Schmadebeck, Nuc. Instr. and Meth. 87, (1970), 37-43.

10. F. W. Stecker, J. I. Vette, and J. I. Trombka, Nature 231, 1971, 122.

11. C. S. Dyer, and G. E. Morfill, Astrophys. and Sp. Sci., 14, 1971, 243.

12. G. J. Fishman, Ap. J. 171, 1972, 163.

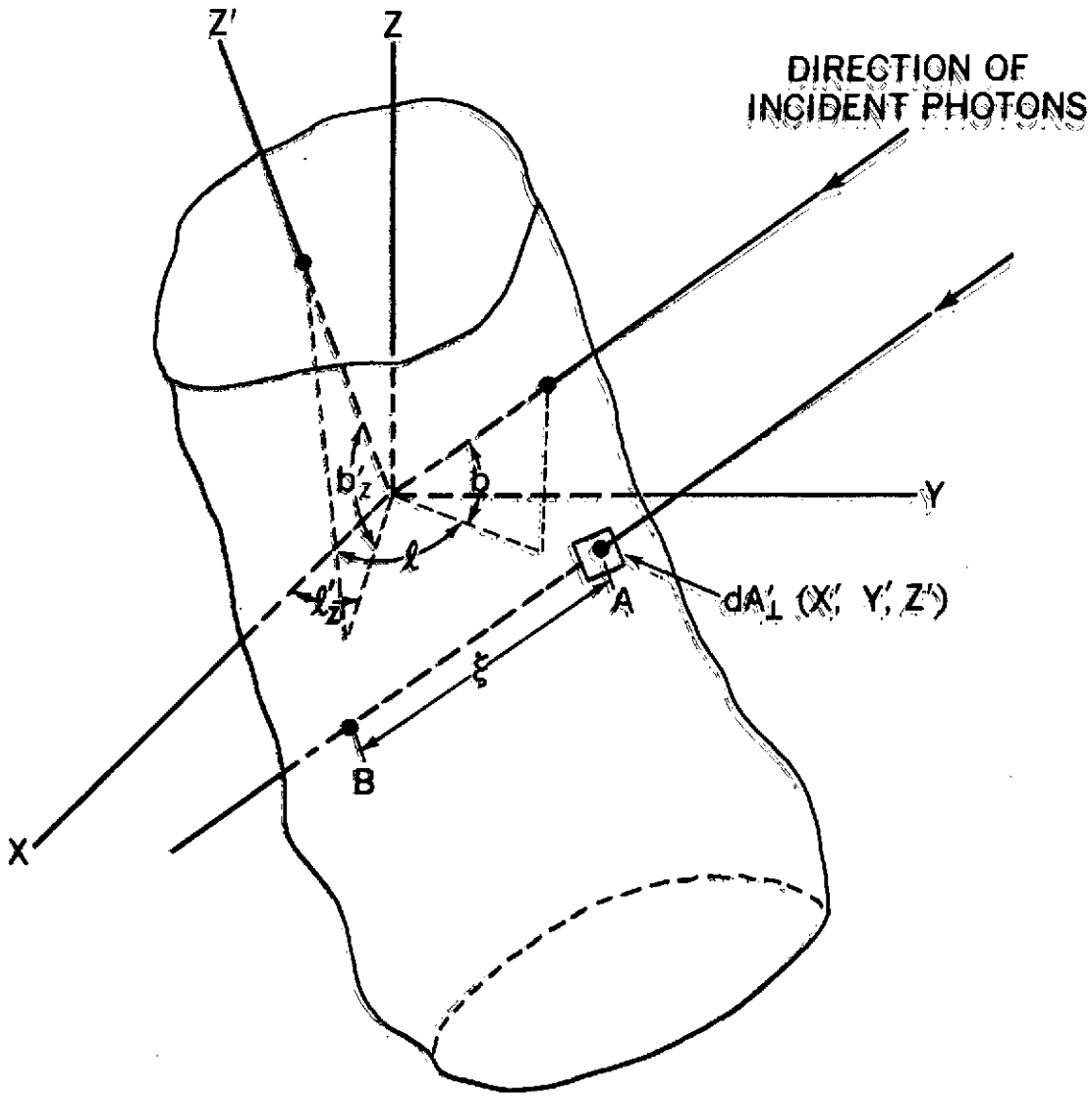

Figure 1. Geometric Configuration for spatially fixed coordinate System (unprimed system) and coordinate system fixed in the detector (primed system).

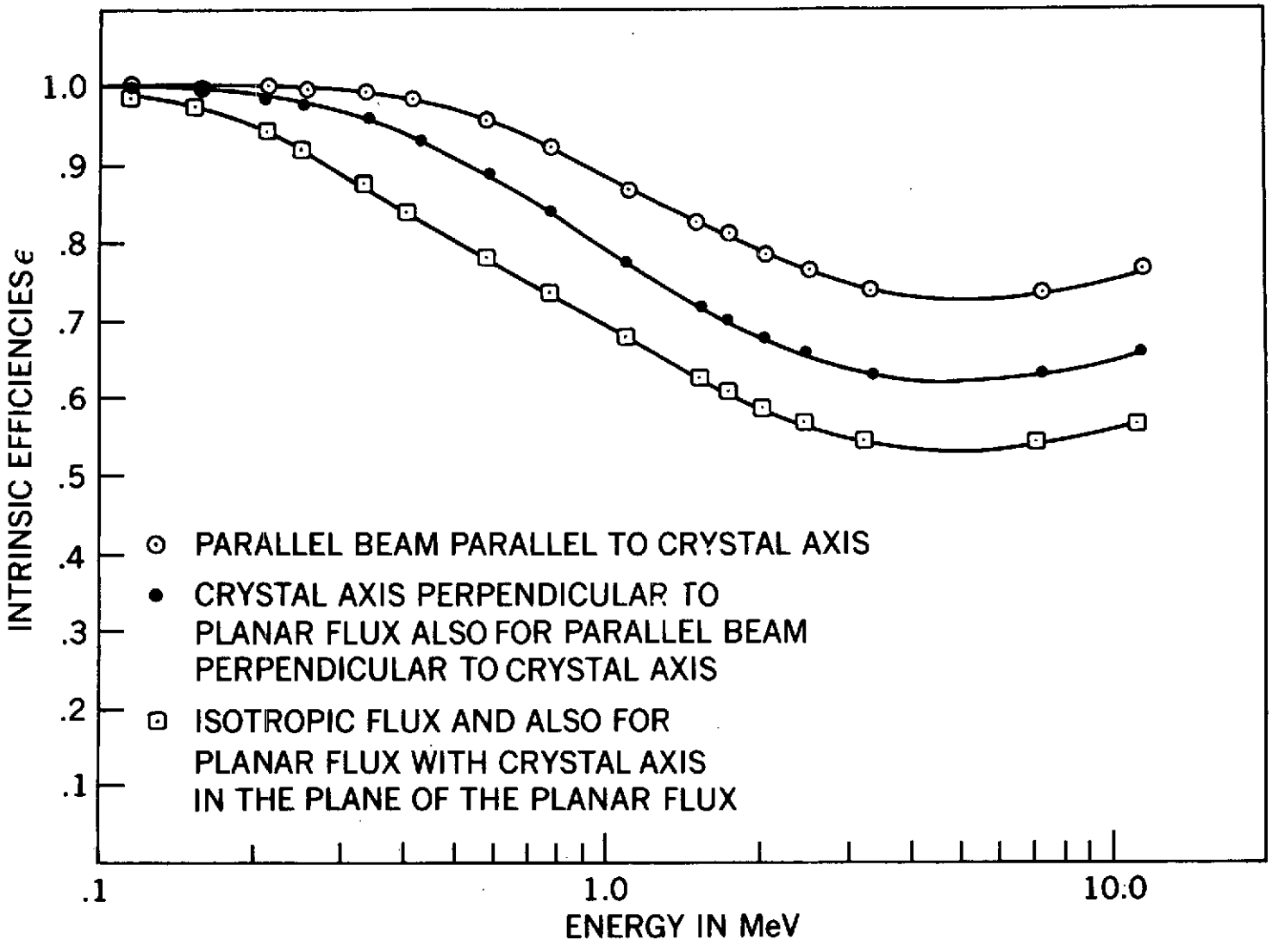

Figure 2. Intrinsic Efficiencies as a Function of Energy for 10.16 cm × 10.16 cm (4" x 4") Cylindrical Crystals.

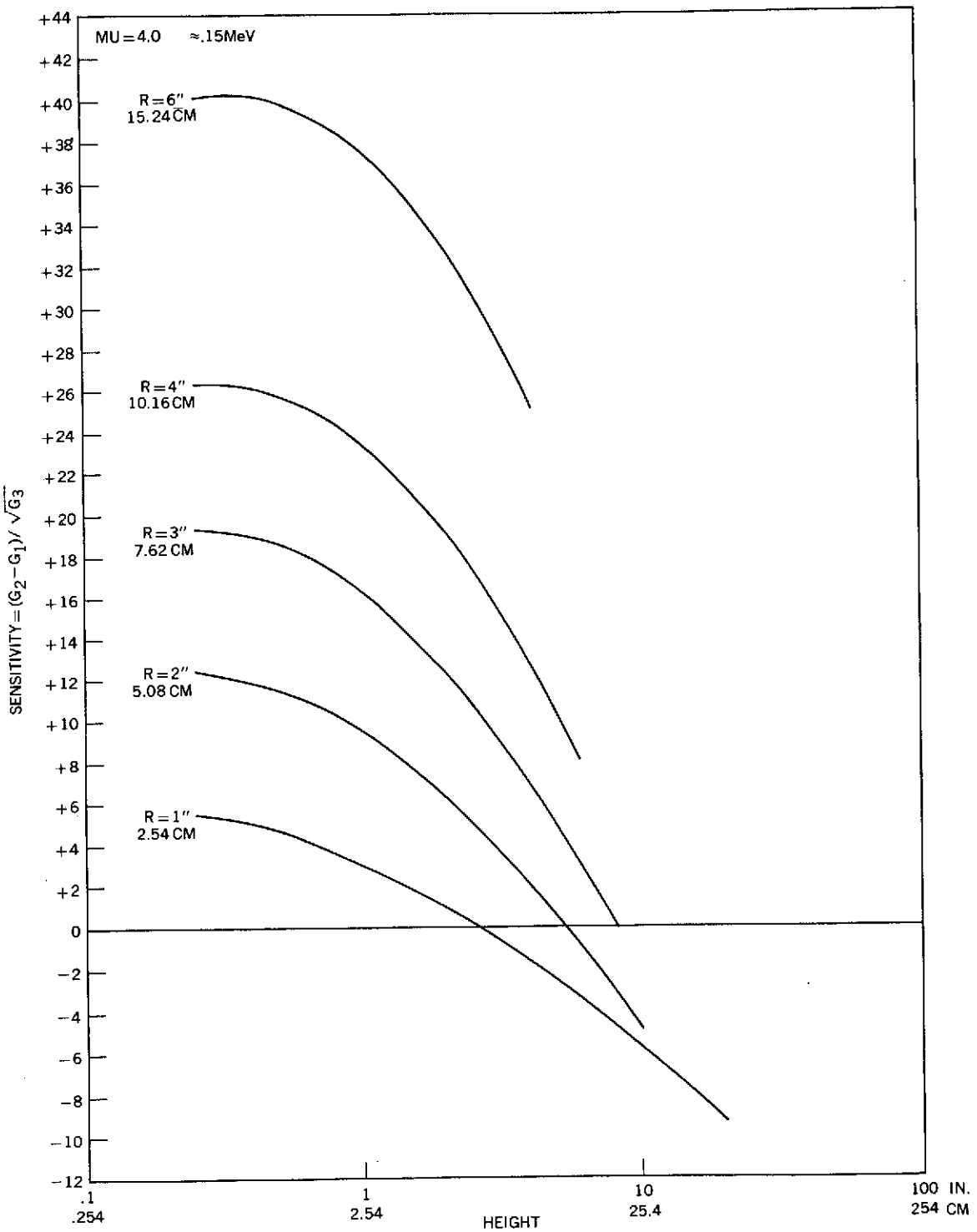

Figure 3. The Sensitivity factor S for CsI as a function of height for a number of crystal radii for $\mu = 4$ ($\sim$ .15 MeV).

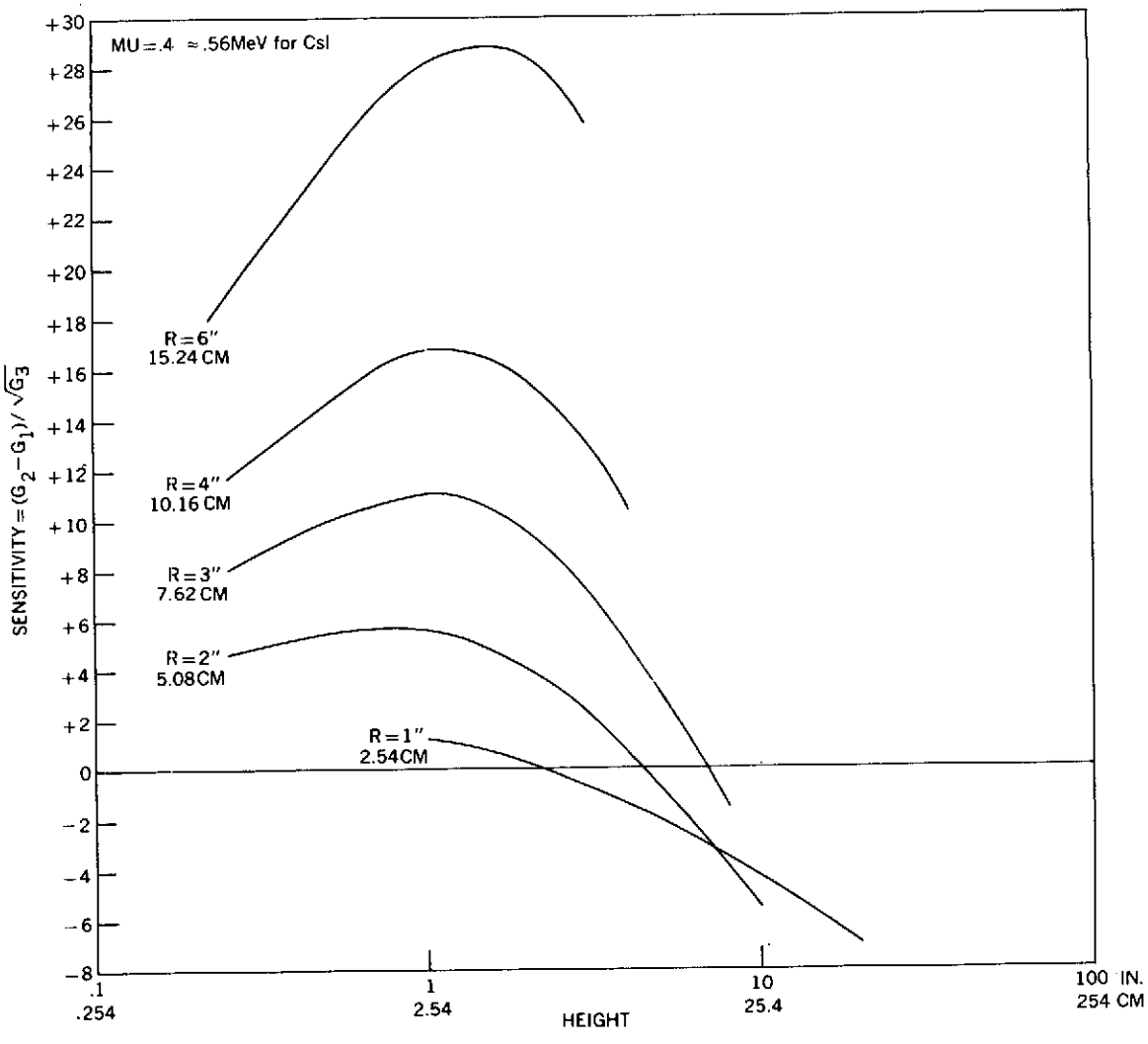

Figure 4. The Sensitivity factor S as a function of height for a number of crystal radii for $\mu = 4$ (~ .56 MeV).

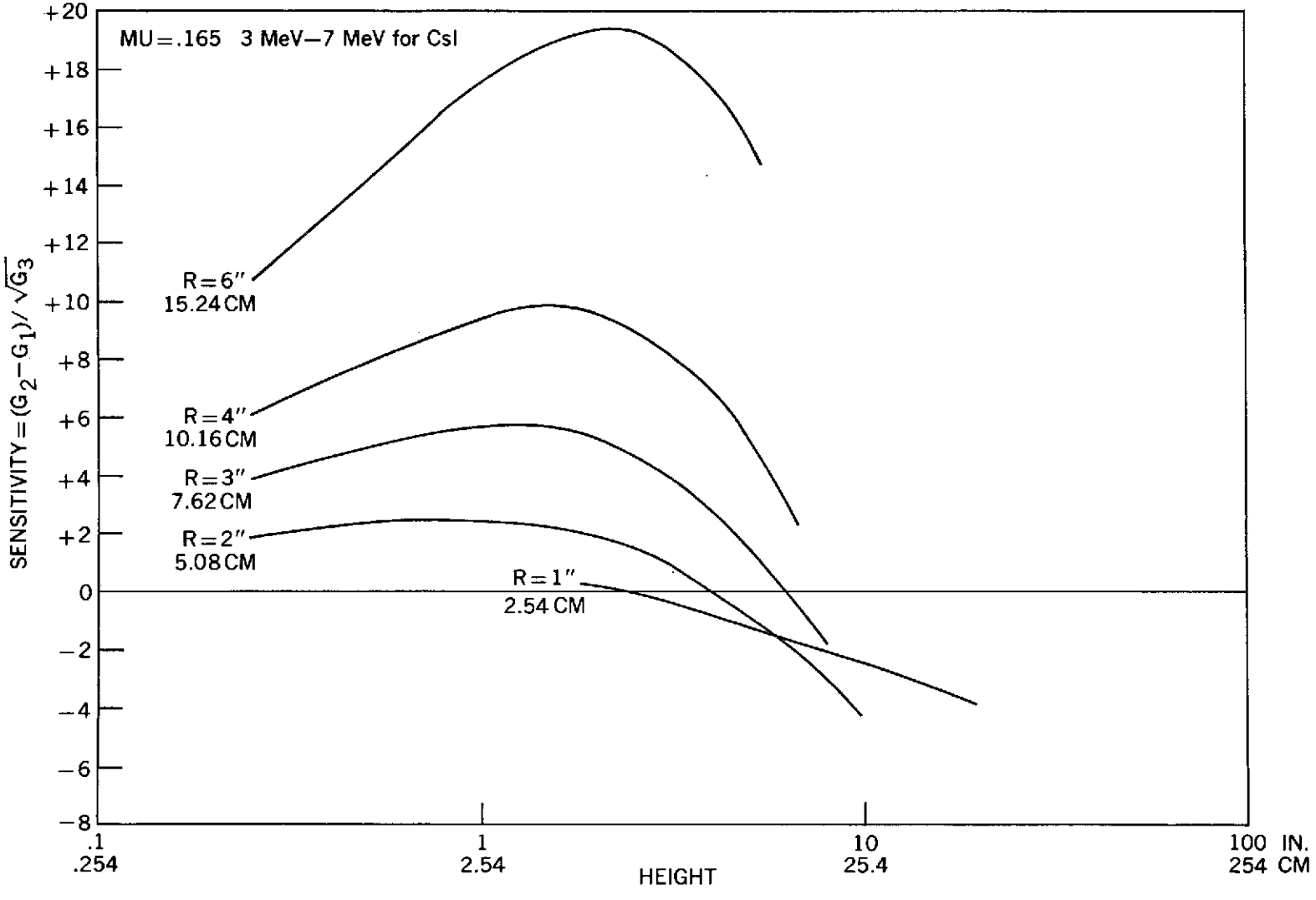

Figure 5. The Sensitivity Factor S for CsI as a function of height for a number of crystal radii for μ =.165 (~ 3 MeV).

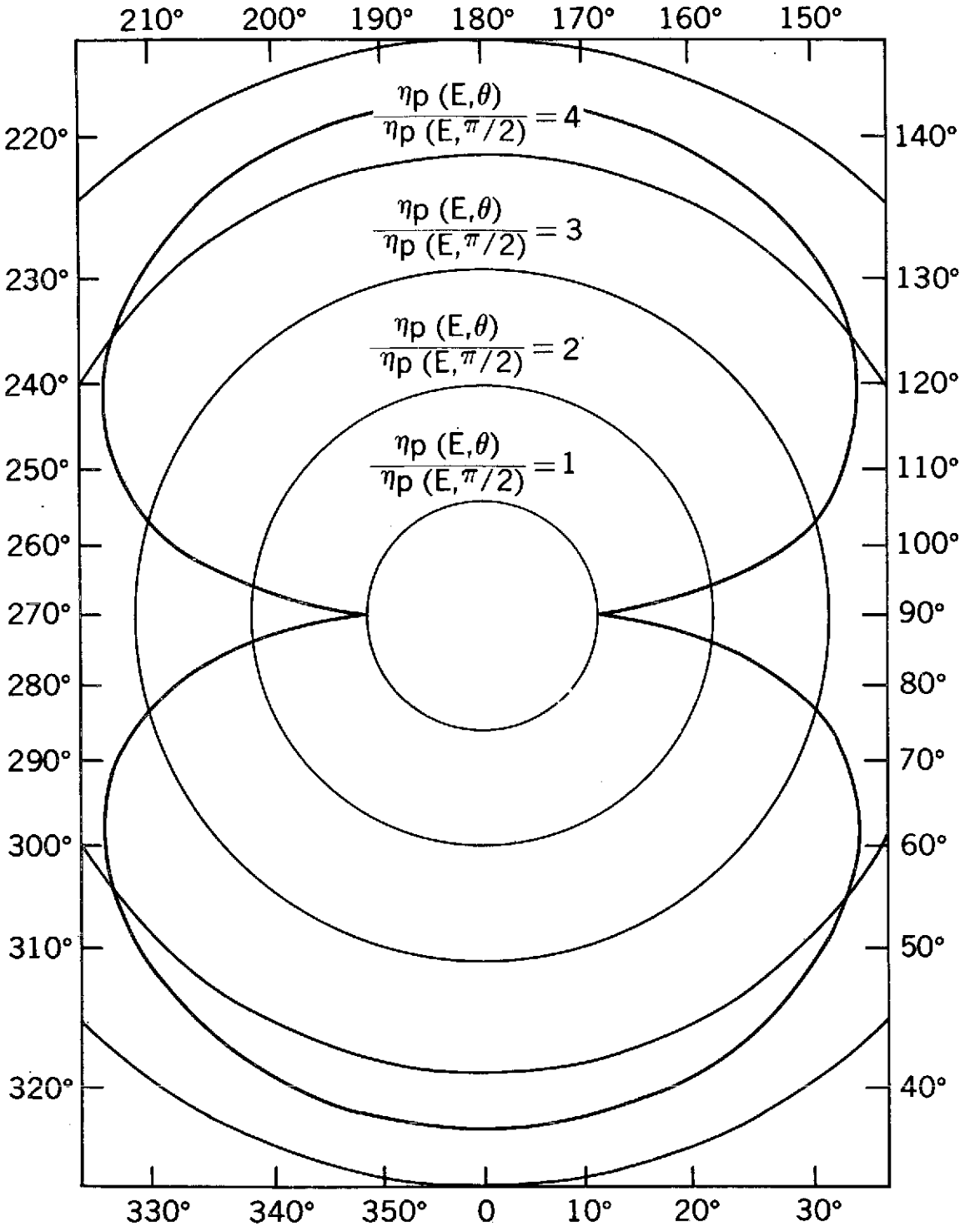

Figure 6. Polar plot of the relative effective detector cross sectional area $\frac{N_p(E,\theta)}{N_p(E,\pi/2)}$ as a function of θ for a 40.62 cm. x 2.54 cm. thick cylindrical CsI crystal and 4 MeV protons.

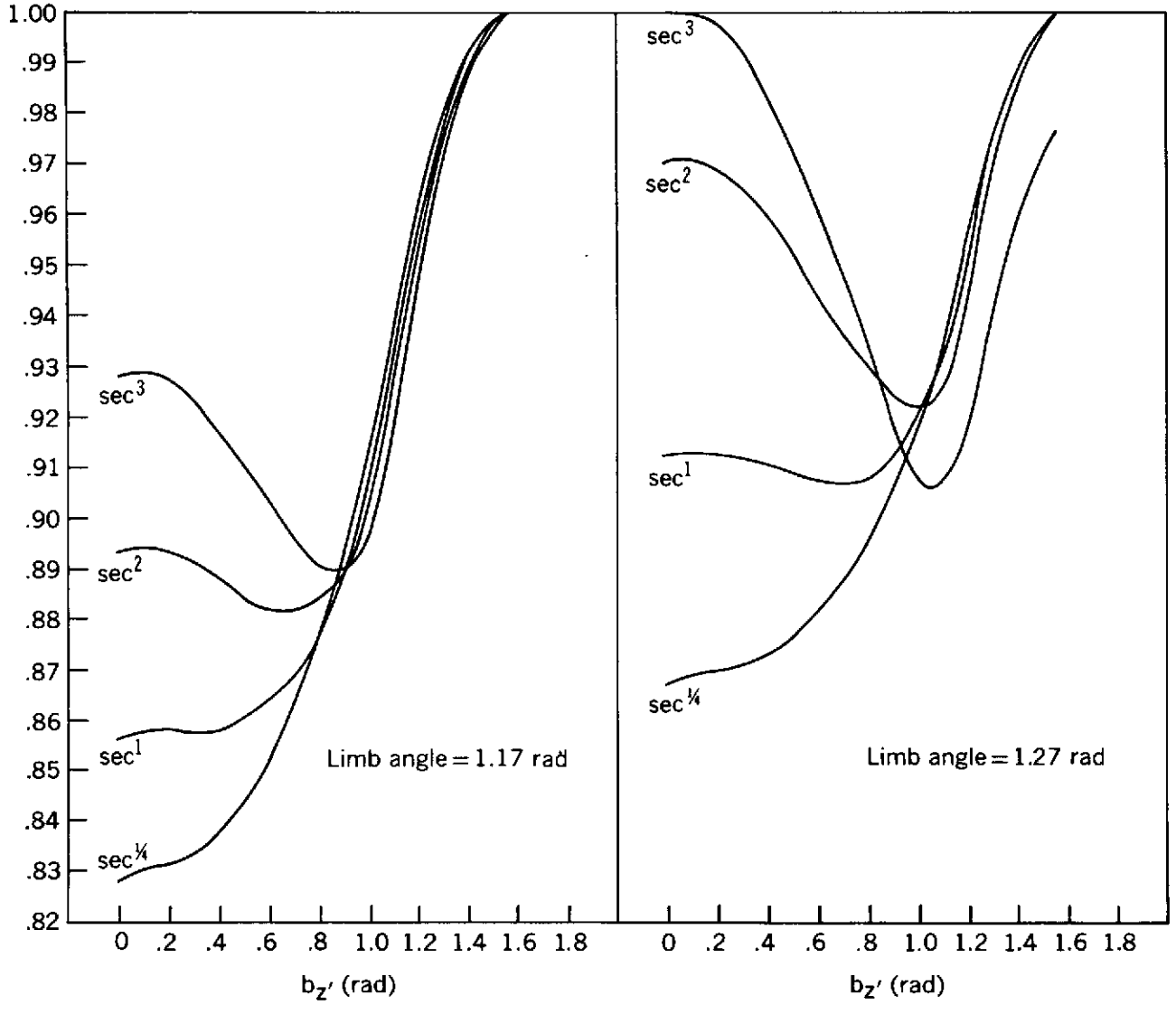

Figure 7. Calculated Counting rate variation relative to maximum as a function of detector orientation in atmospheric albedo; 8.89 cm rad x 2.5 cm thick crystal, 1.5 MeV gamma rays.